JOURNAL OF PHYSICAL ORGANIC CHEMISTRY
J. Phys. Org. Chem. 2002; **15:** 287–292
Published online in Wiley InterScience (www.interscience.wiley.com). DOI: 10.1002/poc.480

Molecular structure effects on the kinetics of hydroxyl radical addition to azo dyes

Hugo Destaillats,[1] Adrián G. Turjanski,[2] Darío A. Estrin[2] and Michael R. Hoffmann[1]*

[1]W. M. Keck Laboratories, California Institute of Technology, Pasadena, California 91125, USA
[2]Departamento de Química Inorgánica, Analítica y Química Física, INQUIMAE, Facultad de Ciencias Exactas y Naturales, Universidad de Buenos Aires, Pabellón 2, Ciudad Universitaria, C1428EHA Buenos Aires, Argentina

Received 19 November 2001; revised 2 January 2002; accepted 17 January 2002

epoc

ABSTRACT: The effect of the molecular structure of azobenzene and related azo dyes on their reactivity towards ·OH radicals in water was investigated by performing ultrasonic irradiation experiments on their aqueous solutions and density functional theory (DFT) calculations. Sonolysis of azobenzene, methyl orange, *o*-methyl red and *p*-methyl red was performed at a frequency of 500 kHz and 50 W applied power under air saturation. Under such irradiation conditions, these molecules were shown to decompose through ·OH radical addition reactions taking place in the bulk liquid. The *ortho* isomer of methyl red reacted at significantly higher rates (nearly 30% higher) than the other three studied compounds in non-buffered aqueous solutions. In contrast, measurements performed at lower pH (10 mM HNO_3), at which the carboxylic group vicinal to the azo group is protonated, yielded a similar reaction rate for all four substrates, i.e. the specific acceleration observed in the *ortho*-substituted dye disappeared with protonation. These results were rationalized by the computation of formation energies of the adduct originated in the ·OH addition to the azo group, performing DFT calculations combined with the polarized continuum model (PCM) of solvation. The calculations suggest that intramolecular H-bonding in the *o*-methyl red–OH adduct provides extra stabilization in that particular case, which correlates with the observed higher addition rates of ·OH radical to the anionic form of that isomer in non-buffered solutions. On the other hand, the energy changes calculated for the ·OH addition to an *o*-methyl red molecule which is protonated in the carboxylic group (representative of the situation at pH 2) do not differ significantly from those computed for the other three molecules studied. Copyright © 2002 John Wiley & Sons, Ltd.
Additional material for this paper is available from the epoc website at http://www.wiley.com/epoc

KEYWORDS: azo dyes; hydroxyl radical addition; kinetics; molecular structure

INTRODUCTION

Hydroxyl radicals participate in several chemical reactions involved in advanced oxidation processes (AOPs) in aqueous media, such as semiconductor photocatalysis,[1] ultrasonic irradiation[2–4] and gamma radiolysis,[5] as well as in more classical techniques such as ozonation[6] and Fenton's reaction.[7] These active species react readily with most organic solutes in water, usually at diffusion-controlled rates.[8] Some experimental information is available on the kinetics and pathways of ·OH radical reactions with azo dyes in aqueous solution.[3,4,9,10] Azo dyes constitute an important group of pollutants present in industrial wastewater effluents. Our recent investigations suggested that ·OH (aq) addition to the azo double bond can be considered the first step of a degradative sequence of reactions under ultrasonic irradiation, that results in the ultimate breakage of the N=N bond and the production of single-ring aromatic byproducts and reaction intermediates.[3] Under continuous sonication, some of these undergo further oxidation to yield carboxylic acids and stable mineralization products such as NO_3^- (aq) and CO_2 (g). Hydroxyl radicals are also able to attack the aromatic rings and the dimethylamino groups in these molecules. Small amounts of byproducts of the latter reaction were detected in the work mentioned.[3]

In our previous studies,[3,4] four model azo compounds were studied: azobenzene (AB) and the dyes methyl orange (MO), *o*-methyl red (*o*-MR) and *p*-methyl red (*p*-MR) (Fig. 1). The presence of a carboxylic group in the vicinity of the azo double bond of *o*-MR is most likely the reason for the observed significantly higher rate of decomposition of that particular dye, as compared with those determined for its isomer *p*-MR and for the related MO and AB. In the last three molecules, the measured rate constants were very similar, indicating a certain insensitivity to the presence of substituents located far from the azo nucleus. The same trend was observed in

**Correspondence to:* M. R. Hoffmann, W. M. Keck Laboratories, California Institute of Technology, Pasadena, California 91125, USA.

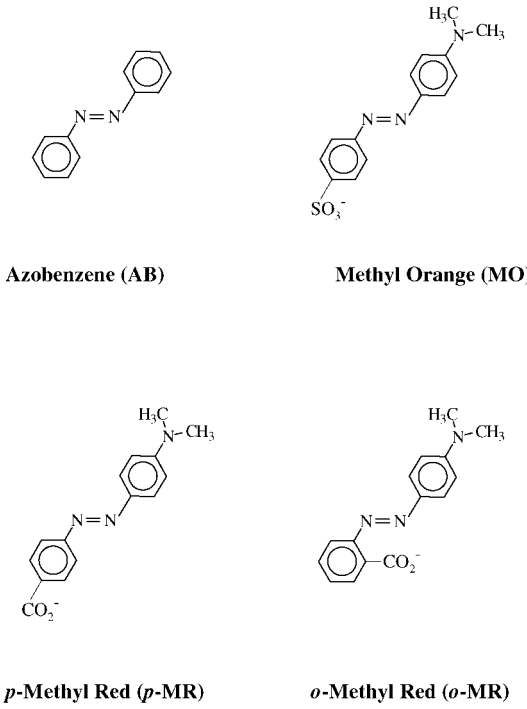

Figure 1. Schematic structures of the dyes studied

experiments performed under different background gases (Ar, O_2 and air). Two other independent determinations of the bimolecular rate constants for the reaction of AB or MO with ·OH radical, based on the pulsed radiolysis of N_2O-saturated dye aqueous solutions, also yielded near by identical values (2.0×10^{10} l mol^{-1} s^{-1}) for these two dyes.[9,10]

In this work, our goal was to provide insight into the influence of the molecular structure on the reactivity of azo compounds towards ·OH radicals in aqueous solution, with the primary aim of explaining the observed rate enhancement due to *ortho* substitution with a carboxylic group. Reactions of organic molecules with ·OH radicals occurring at near diffusion-controlled rates in aqueous solutions present small, albeit non-negligible, activation energies, of the order of 10–20 kJ mol^{-1}.[8,11] The observed reaction rates may differ between different isomers of the reactant owing to changes in their molecular structure.[8,12–14]

In order to understand better the role of the substitution with carboxylic groups, we have extended the available experimental information from near-neutral solutions to the acidic range. The ultrasonic irradiation of solutions of all azo compounds was performed under non-buffered conditions and at pH 2, with all other experimental parameters mantained constant (e.g. ultrasonic frequency, power density, temperature) at the previously reported values.[3] At pH 2, MO and the MRs are present as neutral non-ionic molecules, whereas at even lower pH the cationic species predominate owing to the protonation of N atoms either at the tertiary amino group or in the azo group.[15–18] Under ultrasonic irradiation at frequencies in the range 20–1000 kHz, cavitation bubbles are produced in the liquid. These bubbles are able to couple with the acoustic field and collapse violently during sonication, reaching extreme local conditions of temperature and pressure (in the range of thousands of kelvin and hundreds of bars, respectively). Several chemical processes take place upon cavitation bubble collapse.[19] When the solutes are non-volatile, which is the case with azo dyes, water thermolysis is the main sonochemical reaction taking place in the cavities. The main oxidant species released in solution by this process are ·OH radicals, superoxide and H_2O_2. The former is short-lived, reaching a steady-state concentration in water, while superoxide and H_2O_2 accumulate in the vessel during irradiation. Organic solutes reacting fast with superoxide (such as benzoquinone) were shown to follow zero-order kinetics,[4] while those reacting faster with ·OH radicals follow first-order kinetics. That was observed with azobenzene and azo dyes.[3]

Supporting our experimental studies, we have explored the chemistry of addition of ·OH radical to each of the substrates (i.e. adduct formation), using density functional theory (DFT) calculations[20,21] combined with a continuum model of solvation.[22] In the case of *o*-MR and *p*-MR, both the anionic structure and the protonated molecule were analyzed with the same methodology. The azo dyes studied are present in solution in two different configurations, *cis* (*Z*) and *trans* (*E*),[14] with the latter being the most stable and abundant isomer. Therefore, the calculations performed in this work focus on the comparison between *trans* isomers only.

EXPERIMENTAL

The experimental setup and methodology employed in the sonochemical experiments have been described previously.[3,4] Ultrasonic irradiation of air-saturated solutions of the four substrate molecules in water and in 0.01 M HNO_3 (aq) was performed in a 650 ml batch sonoreactor (Undatim Ultrasonics), operating at 50 W (77 W l^{-1} power density). The pH of the solutions was measured with an Altex 71 pHmeter, before and after ultrasonic irradiation. In the case of non-buffered solutions, the pH changed from an initial value of 6.5 to a final reading near to 5.0. When HNO_3 was employed to control the pH, the initial value was set at 2.0 and it remained constant during the 30 min of irradiation. The initial concentration of the substrates was adjusted over the range of 2.7–3.2 μM. These values are close to the highest soluble dye concentrations attainable at pH 2, owing to the precipitation of the non-ionic organic molecules. Such solubility limitations did not exist during our previous experiments in non-buffered solutions, where the anionic forms of the dyes readily dissolved in water, and therefore the concentrations

previously employed (10 μM) were impossible to reach at pH 2. For that reason, we repeated our previous experiments (in near-neutral conditions) reducing the initial dye concentration to 3 μM, for the sake of comparison. The solutions were filtered through 0.45 μm pore size filters (Gelman) prior to sonication. The temperature of the treated solutions was kept constant at 15.0 °C by circulating water from a thermostat through the cooling jacket of the reactor. Samples (1 ml) were withdrawn at different times and analyzed with a Hewlett-Packard 8452 A diode-array spectrophotometer, using a semi-micro 10 mm quartz cuvette.

The chemical reagents, AB (Aldrich, >99%), MO (Baker, >95%), *o*-MR (Sigma, >95%) and *p*-MR (Sigma, >97%) were used without further purification. Solutions were prepared with water purified using a Millipore Milli-Q UV Plus system (R = 18.2 MΩ cm).

Computational methodology

The geometry of AB, MO, *o*-MR and *p*-MR (the MRs in their anionic and protonated forms) and their corresponding ·OH aducts were fully optimized without symmetry constraints using DFT calculations.[20,21] Restricted RHF calculations were performed for closed-shell species, and an unrestricted scheme was employed for the radical states.

The DFT calculations were performed using a Gaussian basis set implementation of DFT.[21] The Kohn–Sham self-consistent procedure was applied for obtaining the electronic density and energy through the determination of a set of one-electron orbitals.[20] Gaussian basis sets were used for the expansion of the one-electron orbitals and also for the additional auxiliary set used for expanding the electronic density. Matrix elements of the exchange-correlation potential were calculated by a numerical integration scheme.[23] The orbital and auxiliary basis sets optimized by Sim and coworkers[24] for DFT calculations were used for C, N and H atoms. The contraction patterns were (5211/411/1) for C and N and (41/1) for H. The contraction patterns for the electron density expansion sets were (1111111/111/1) for C and N and (111111/1) for H. A more detailed description of the technical aspects of the program is given in Ref. 21 The generalized gradient approximation (GGA) Becke and Perdew combination of functionals for exchange and correlation, respectively, was employed.[25,26]

Solvent effects in DFT calculations were modeled using the polarized continuum model (PCM) schemes. The PCM implementation given in Ref. 22, in which the self-consistency between the solute wavefunction and solvent polarization is achieved during the self-consistent field cycle, was employed. PCM computations were performed using the Gaussian98 software package at the optimized geometries in vacuum.[27]

RESULTS AND DISCUSSION

Sonolysis of azobenzene and azo dyes in aqueous solution

The sonochemical depletion rates of AB, MO, *o*-MR and *p*-MR were determined in water and in 0.01 M HNO_3 aqueous solutions. The bleaching rates of the substrates were studied following the disappearance of the parent molecule through its absorbance at λ_{max} in the visible region. Dye bleaching reactions followed pseudo-first-order rates in every case. Under acidic conditions, the anionic dyes are present in the protonated (i.e. non-ionic) forms exclusively, whereas azobenzene remains unchanged.[15–18] Except for AB, the spectra of the protonated molecules are red shifted and considerably more intense than those corresponding to the anionic species.[28,29] The values of the measured pseudo-first-order rate constants (k_{-X}) in each case, together with the corresponding spectroscopic information, are reported in Table 1.

The results obtained in non-buffered solutions are essentially the same as those obtained in our previous work for higher initial concentrations of the dyes, the rate measured for *o*-MR (k_{-o-MR}) being higher than the others by about 30%. As opposed to the trends previously observed for the sonolysis rates of anionic species, the experiments at low pH indicate that protonated *o*-MR molecules are not substantially more reactive towards ·OH radicals than the other molecules. Within experimental error, all four reported k_{-X} values are essentially the same. Figure 2 illustrates the ratio of the observed degradation rate of X = MO, *o*-MR and *p*-MR over the value determined for AB under the same experimental conditions. Whereas the experiments performed at pH 2 do not show any particular reactivity enhancement as compared with AB, the data for non-buffered solutions illustrate the significantly higher relative rate measured for *o*-MR, which is not observed with the other studied substrates.

The actual values of the measured rate constants are higher at pH 2 than in near-neutral solutions. This difference is probably related to the presence of a significant concentration of HNO_3 in the former case, which may participate in a variety of high-temperature gas-phase reactions within the cavitation bubbles, particularly

$$HONO_2(g) \xrightarrow{\Delta} {}^{\cdot}OH\ (g) + {}^{\cdot}NO_2(g) \qquad (1)$$

Changes in the gaseous composition of cavitation bubbles affect the sonochemical rates due to physical and chemical modifications of the implosion conditions.[3,4,19] Under the bubble collapse conditions at pH 2 in the presence of HNO_3, a higher yield of available ·OH radicals may result. This enhanced flux will ultimately

Table 1. Observed pseudo-first-order rate constants (k_{-X}) for the sonolysis under air saturation, bimolecular rate constant for the reaction of each dye with OH radicals (k_{-X}^{OH}) and spectroscopic parameters for X = AB, MO, *o*-MR and *p*-MR

pH	Parameter	AB	MO	*o*-MR	*p*-MR
Non-buffered[a]	λ_{max} (nm)	319	464	430	464
	ε_{max} (l mol^{-1} cm^{-1})	22000	26900	20900	26300
	$10^3\ k_{-X}$ (min^{-1})	42 ± 2	43 ± 2	55 ± 2	40 ± 2
	$10^{-10}\ k_{-X}^{OH}$ (l mol^{-1} s^{-1})	2[c]	2.0 ± 0.1	2.6 ± 0.1	1.9 ± 0.1
2[b]	λ_{max} (nm)	319	507	520	508
	ε_{max} (l mol^{-1} cm^{-1})	23900	45700	51800	44500
	$10^3\ k_{-X}$ (min^{-1})	82 ± 3	85 ± 3	83 ± 3	88 ± 3
	$10^{-10}\ k_{-X}^{OH}$ (l mol^{-1} s^{-1})	2[c]	2.1 ± 0.1	2.0 ± 0.1	2.1 ± 0.1

[a] $[OH(aq)]_{ss} = (3.5 \pm 0.2) \times 10^{-14}$ M
[b] $[OH(aq)]_{ss} = (6.9 \pm 0.2) \times 10^{-14}$ M
[c] Literature value,[a] taken as reference.

reach the bulk solution and subsequently react with the azo dyes at a higher pseudo-first-order rates. The experimental pseudo-first-order rate constant for the depletion of the substrate X, k_{-X}, can be expressed as the product of the bimolecular rate constant for the reaction of X with ·OH radicals (k_{-X}^{OH}) times the steady-state ·OH radicals concentration attained in the bulk liquid during ultrasound irradiation, $[^{\cdot}OH\ (aq)]_{ss}$, as follows:

$$k_{-X} = k_{-X}^{OH}[^{\cdot}OH\ (aq)]_{ss} \quad (2)$$

Replacing with the data for AB, for which the bimolecular rate is known ($k_{-AB}^{OH} = 2 \times 10^{10}$),[9] we can estimate $[^{\cdot}OH\ (aq)]_{ss}$ under the two regimes. These values are reported in Table 1, and suggest that HNO_3 increases the available concentration of ·OH radicals by a factor of nearly 2. The determination of $[^{\cdot}OH\ (aq)]_{ss}$ in non-buffered solutions is also in good agreement with our previous determinations in the same reactor.[4] Equation (2) allows us to estimate the bimolecular rate constants k_{-X}^{OH} for MO, *o*-MR and *p*-MR under the two pH conditions, also reported in Table 1.

We have assumed, in the present analysis, that only ·OH radicals are able to decolorize azobenzene and azo dyes solutions under ultrasonic irradiation. Reactions involving sonochemically generated H_2O_2 are slower, and can be neglected. Superoxide and $^{\cdot}O_2H$ radicals are also produced during sonolysis. However, when these species react with the substrate at rates similar to those of ·OH (diffusion controlled), overall zeroth-order kinetics should be observed.[4] Therefore, the observation of first-order degradation kinetics in this case indicates that ·OH radicals are the primary bleaching agents, and that the other radical species are of minor importance in the overall process.

Computational study of ·OH addition to azo compounds

The optimized structures for the adducts are presented in Fig. 3 and the most relevant geometric parameters are reported in Table 2. In all cases, a significant increase in the N—N bond distance is observed upon formation of the adduct; this is consistent with the formally single N—N bond in the latter. These results for the azo compounds agree with previous DFT calculations of substituted azobenzenes,[30] and are consistent with the observed products of their sonolysis, which are mostly single-ring aromatic compounds originated in the breakage of the azo bond.[3] A unique differentiating feature in the structure of the *o*-MR adduct, compared with the other three, is that the O—H bond is partially dissociated due to the H-atom abstraction by the carboxyl group. The O—H distance in this case is 1.380 Å, compared with values corresponding to typical ·OH bonds in the cases of AB, MO and *p*-MR, which are close to 1 Å. The N—O bond distance is also significantly shorter in the *o*-MR adduct than in the other species. In the case of protonated *o*-MR, there is still an H-bond, but since it is much weaker than in the unprotonated case, the O—H bond length increases by only 0.05 Å with respect to typical ·OH values. The intramolecular H-bonding is facilitated by the formation of a seven-membered ring, which includes the ·OH, one N atom at the azo group, two aromatic carbons and a C—O bond from the carboxyl group.

In all cases, the spin density of the adducts is mainly localized on the nitrogen atoms of the azo group, and on the *para* and *ortho* carbon atoms of the aromatic ring next to the N where the hydroxyl radical is not bonded. As an illustrative example, in *o*-MR the Mulliken spin populations of the N atom bonded to the hydroxyl radical, the other N atom and the *ortho* and *para* carbons are 0.15, 0.31, 0.10 and 0.10, respectively.

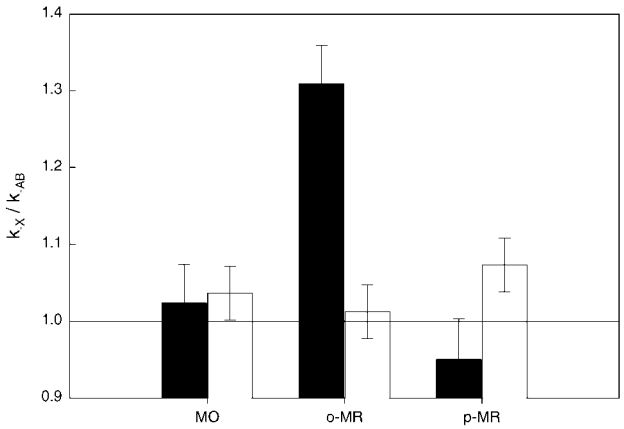

Figure 2. Ratio between the determined pseudo-first-order rate constants (k_{-X}) for the sonolysis of MO, *o*-MR and *p*-MR and for azobenzene (k_{-AB}) under air saturation in non-buffered solutions (black) and at pH 2 (white)

Table 2. DFT optimized selected geometric parameters for OH addition products

Parameter	AB	MO	*o*-MR	*o*-MR prot.	*p*-MR	*p*-MR prot
d(NN) (Å)[a]	1.274	1.282	1.282	1.276	1.283	1.278
d(NN) (Å)	1.317	1.339	1.334	1.323	1.329	1.325
d(OH) (Å)	0.988	0.989	1.380	1.033	0.989	0.989
d(NO) (Å)	1.439	1.450	1.336	1.388	1.445	1.452
∠NOH (°)	103.8	105.0	103.6	102.7	104.3	102.0

[a] These correspond to the reactant.

Table 3. Energetic changes (kcal mol^{-1}) (1 kcal = 4.184 kJ) in vacuum and aqueous solution for reaction (3)

	AB	MO	*o*-MR	*o*-MR prot.	*p*-MR	*p*-MR prot
DFT	−16.5	−11.8	−42.1	−22.3	−14.1	−16.4
DFT/PCM	−11.3	−6.4	−22.8	−16.1	−10.0	−10.4

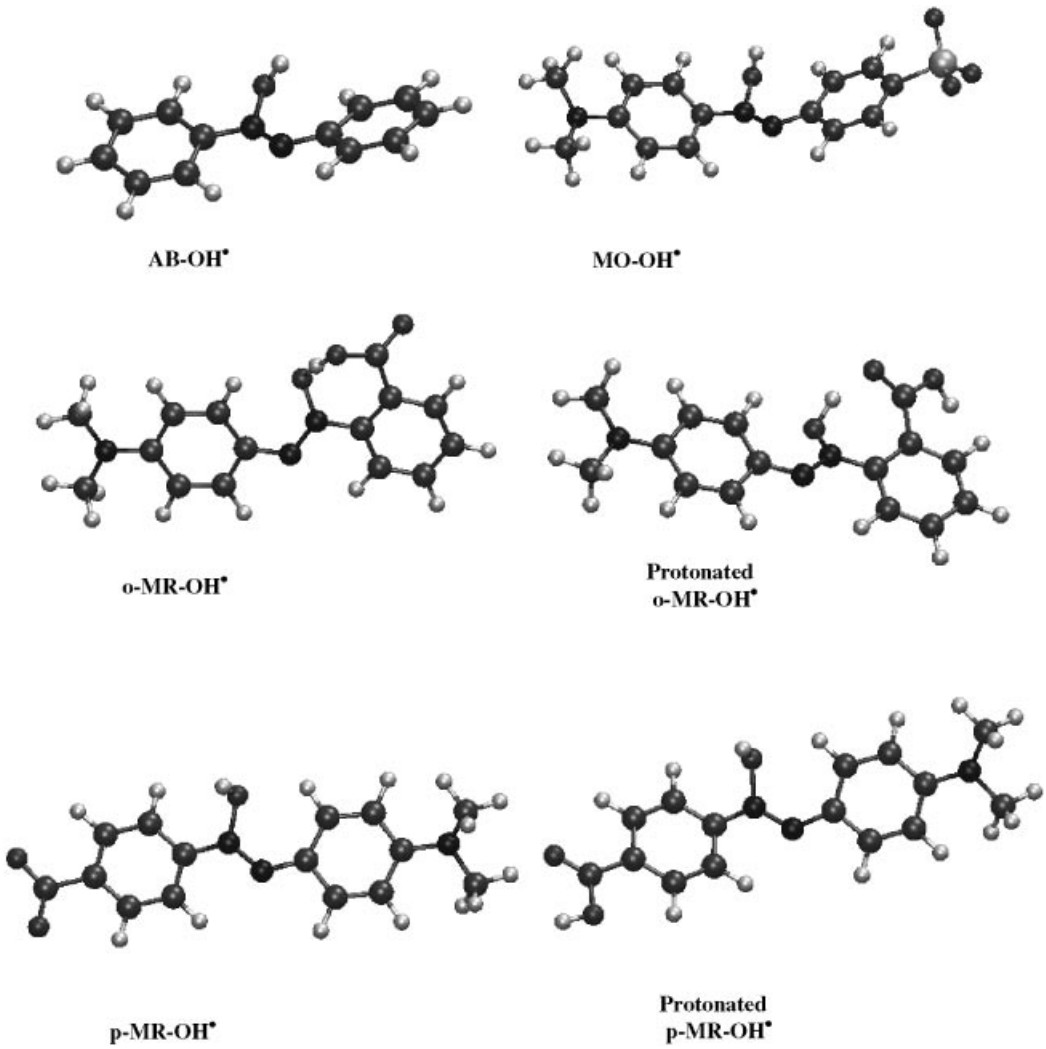

Figure 3. DFT optimized structure of the adducts corresponding to the four dyes and the protonated forms of *o*-MR and *p*-MR

Table 3 illustrates the calculated values for the energetic change ΔE associated with the addition of $^{\cdot}OH$ radical to the azo double bond of each substrate molecule:

$$X + {}^{\cdot}OH \rightarrow {}^{\cdot}X\text{---}OH \qquad (3)$$

where X = AB, MO, *o*-MR or *p*-MR (the MRs in their anionic and protonated form). It can be seen that for all species the process is predicted to be exergonic in vacuum. AB, *p*-MR, the protonated *p*-MR and MO yield very similar results. On the other hand, ΔE calculated for *o*-MR is significantly higher. This is consistent with the experimental kinetic observation, if more negative values for ΔE are associated with smaller activation energies. A significant difference between *o*-MR and the other azo species is due to the fact that a very strong intramolecular hydrogen bond is formed upon $^{\cdot}OH$ addition in this particular case. Upon protonation of *o*-MR there is a marked decrease in ΔE; however, the computed value is still much larger than those corresponding to the other azo compounds. This is also due to the formation of an intramolecular H-bond (Fig. 3). The decrease in ΔE can be ascribed to the fact that for unprotonated *o*-MR, the hydrogen bond formed with the negatively charged carboxylic group is much stronger than that formed with the neutral protonated moiety. Protonation has a very small effect on the only other azo compound, *p*-MR, containing a carboxylic group, since in this case H bonds are not formed upon reaction with $^{\cdot}OH$.

In the case of AB, *p*-MR and MO, consideration of solvent effects leads to a decrease in the computed energy changes. This can be understood in terms of a reduction in solvation energies on going from the reactants to the adduct. It is interesting that the decrease is of the order of magnitude of the energy associated with a hydrogen bond (4–5 kcal mol^{-1}), which is expected to be lost when free $^{\cdot}OH$ forms the corresponding adduct. In the case of *o*-MR, the reduction in ΔE due to solvent effects is of the order of 20 kcal mol^{-1}. In this situation, both reactants, $^{\cdot}OH$ and *o*-MR, form strong H-bonds with the solvent; these interactions are subsequently lost upon formation of the adduct. It is interesting that in the case of the protonated *o*-MR, a case in which the neutral carboxylic moiety forms weaker H-bonds with the solvent, the trends are similar to those for the other azo compounds.

In summary, there is good agreement between the observed pseudo-first-order rates for the degradation of the dyes and the above calculations of ΔE for the $^{\cdot}OH$ adduct formation with both anionic and non-ionic (protonated) dyes, which strongly suggests that internal H-bonding in the *o*-MR adduct is the cause of the unusually high reactivity of its anionic form.

Acknowledgements

D.A.E. is a member of the National Research Council of Argentina (CONICET).

REFERENCES

1. Kesselman JM, Weres O, Lewis N, Hoffmann MR. *J. Phys. Chem. B* 1997; **101**: 2637–2643.
2. Vinodgopal K, Peller J, Makogon O, Kamat PV. *Water Res.* 1998; **32**: 3646.
3. Joseph J, Destaillats H, Hung H, Hoffmann M. *J. Phys. Chem. A* 2000; **104**: 301–307.
4. Destaillats H, Colussi AJ, Joseph JM, Hoffmann MR. *J. Phys. Chem. A* 2000; **104**: 8930–8935.
5. Ravishankar D, Raju B. *J. Radioanal. Nucl. Chem.* 1994; **178**: 351–357.
6. Hoigne J, Bader H. *Water Res.* 1976; **10**: 377–386.
7. Solozhenko EG, Soboleva NM, Goncharuk VV. *Water Res.* 1995; **29**: 2206–2210.
8. Buxton GV, Greenstock CL, Helman WP, Ross AB. *J. Phys. Chem. Ref. Data* 1988; **17**: 513.
9. Panajkar MS, Mohan H. *Indian J. Chem.* 1993; **32A**: 25.
10. Padmaja S, Madison S. *J. Phys. Org. Chem.* 1999; **12**: 221–226.
11. Mezyk SP. *Can. J. Chem.* 1994; **72**: 1116–1119.
12. O'Neill P, Steenken S, Schulte-Frohlinde D. *J. Phys. Chem.* 1977; **81**: 31–34.
13. Iddon B, Phillips GO, Robbins KE, Davies JV. *J. Chem. Soc. B* 1971; 1887–1892.
14. Cimiraglia R, Hofmann H-J. *Chem. Phys. Lett.* 1994; **217**: 430–435.
15. Sanchez AM, Barra M, Rossi RH. *J. Org. Chem.* 1999; **64**: 1604–1609.
16. Mukherjee S, Bera SC. *J. Chem. Soc., Faraday Trans.* 1998; **94**: 67–71.
17. Tawarah KM, Khouri SJ. *Dyes Pigm.* 1992; **20**: 261–270.
18. Tawarah KM, Abu-Shamleh HM. *Dyes Pigm.* 1991; **17**: 203–215.
19. Colussi AJ, Weavers L, Hoffmann MR. *J. Phys. Chem. A* 1998; **102**: 6927–6934.
20. Kohn W, Sham LJ. *Phys. Rev. A* 1965; **140**: 1133.
21. Estrin DA, Corongiu G, Clementi E. In *METECC, Methods and Techniques in Computational Chemistry*, Clementi E (ed). Stef: Cagliari, 1993; chapt. 12.
22. Cossi M, Barone V, Cammi R, Tomasi J. *Chem. Phys. Lett.* 1996; **255**: 327.
23. Becke AD. *J. Chem. Phys.* 1988; **88**: 1053.
24. (a) Sim F, Salahub DR, Chin S, Dupuis M. *J. Chem. Phys.* 1991; **95**: 4317; (b) Sim F, St-Amant A, Papai Y, Salahub DR. *J. Am. Chem. Soc.* 1992; **114**: 4391.
25. Perdew PW. *Phys. Rev. B* 1986; **33**: 8800; Erratum, *Phys. Rev. B* 1987; **34**: 7406.
26. Becke AD. *Phys. Rev. A* 1988; **38**: 3098.
27. Frisch MJ, Trucks GW, Schlegel HB, Scuseria GE, Robb MA, Cheeseman JR, Zakrzewski VG, Montgomery JA Jr, Stratmann R, Burant J, Dapprich S, Millam JM, Daniels AD, Kudin KN, Strain MC, Farkas O, Tomasi J, Barone V, Cossi M, Cammi R, Mennucci B, Pomelli C, Adamo C, Clifford S, Ochterski J, Petersson GA, Ayala PY, Cui Q, Morokuma K, Malick DK, Rabuck AD, Raghavachari K, Foresman JB, Cioslowski J, Ortiz JV, Baboul AG, Stefanov BB, Liu G, Liashenko A, Piskorz P, Komaromi I, Gomperts R, Martin RL, Fox DJ, Keith T, Al-Laham MA, Peng CY, Nanayakkara A, Gonzalez C, Challacombe M, Gill PMW, Johnson B, Chen W, Wong MW, Andres JL, Gonzalez C, Head-Gordon M, Replogle ES, Pople JA. Gaussian98, Rev. A7. Gaussian: Pittsburgh, PA, 1998.
28. Graselli JD. (ed). *Atlas of Spectral Data and Physical Constants for Organic Compounds*. CRC Press: Cleveland, OH, 1973.
29. Phillips JP, Freedman LD, Cymerman J (eds). *Organic Electronic Spectral Data*, Vol. VI. Wiley–Interscience: New York, 1973.
30. Biswas N, Umapathy S. *J. Phys. Chem. A* 2000; **104**: 2734.